JOURNAL OF AIRCRAFT
Vol. 33, No. 3, May–June 1996

Comparison of F/A-18A Inlet Flow Analyses with Flight Data Part 1

C. Frederic Smith* and Steve D. Podleski†
NYMA, Inc., Brook Park, Ohio 44142-1099
Wendy S. Barankiewicz‡
NASA Lewis Research Center, Cleveland, Ohio 44135-3191
and
Susan Z. Zeleznik§
NYMA, Inc., Brook Park, Ohio 44142-1099

Full Navier–Stokes calculations on the F/A-18A High Alpha Research Vehicle inlet for several angles of attack and freestream Mach numbers have been obtained. The predicted forebody/fuselage surface static pressures agreed well with flight data. The surface static pressures along the inlet highlight region are in good agreement with the numerical predictions. The major departure in agreement is along the bottom of the inlet lip at 30- and 60-deg angle of attack where a possible streamwise flow separation is not predicted by the code. A comparison of the predicted total pressure contours with flight data indicates that the numerical results are within the excursion range of the unsteady data, which is the best the calculations can attain unless an unsteady simulation is performed.

Nomenclature

C_p = $(P - P_\infty)/0.5\rho_\infty V_\infty^2$
FS = fuselage station in full scale inches, 0 at 60.5 in. ahead of nose
$\dot{m}$ = mass flow rate, lbm/s
P = local static pressure, lb/ft^2
P_t = local total pressure, lb/ft^2
$P_{t_{av}}$ = rake-averaged total pressure at engine face, lb/ft^2
$P_{t_{max}}$ = maximum total pressure, lb/ft^2
$P_{t_{min}}$ = minimum total pressure, lb/ft^2
P_{t_∞} = freestream total pressure, lb/ft^2
P_∞ = freestream static pressure, lb/ft^2
s = wingspan, ft
$T_{t_{av}}$ = rake-averaged total temperature at engine face, °R
V_∞ = freestream velocity, ft/s
z = spanwise distance from wing root, ft
α = angle of attack, deg
β = angle of yaw, deg
δ = $P_{t_{av}}/14.696$ lb/in.^{2}
θ = $T_{t_{av}}/519$°R
ρ_∞ = freestream density, slug/ft^3

Introduction

THE F/A-18A aircraft has experienced engine stalls at high angles of attack and yaw flight conditions that were outside of its flight envelope. At these flight conditions, high angular rates were also present. Future fighter aircraft may be designed to operate routinely in this expanded flight regime. Therefore, it is essential that an understanding of the inlet flowfield at these flight conditions be obtained. This work is part of a larger program discussed in Ref. 1. Because of the complex interactions of the fuselage flowfield and the inlet flowfield, a study of the flow within the inlet must also include external effects. Past calculations of flow about the F/A-18A have not included the inlet and ramp.[2,3] These features are usually fared over and assumed not to influence the external flowfield significantly. However, the effects from the upstream forebody, leading-edge extension (LEX) and diverter must be included to provide the proper inflow conditions to the inlet duct.

The results of including the inlet and ramp in the flow simulation are reported in Ref. 4. The results were used to refine the grid and geometry definition. The results obtained with this revised simulation are reported in Ref. 5. The current work was performed to prepare for computing the flowfield within the F/A-18A High Alpha Research Vehicle inlet and evaluating the results with flight data. These calculations were performed ahead of the tests. The early calculations were used to define some of the instrumentation requirements for the flight tests.

In Part 1 of this article, full Navier–Stokes (FNS) calculations are presented for 30- and 60-deg angle of attack and zero sideslip. Part 2 will discuss nonzero sideslip results.[6] The freestream Mach number is 0.3 and the altitude is 25,000 ft. Flight data consist of surface pressures along the forebody/LEX, inlet highlight, and duct around the engine face plane. In addition, time-averaged and unsteady total pressures were measured at the engine face. The forebody/LEX experimental static pressures were obtained from Ref. 7. Previous studies[8,9] contain a limited amount of experimental data. One aspect of particular distinction with this current test program is the amount of unsteady data available for analysis that sheds some light on the ability of asymptotic analysis codes to capture the essential flow physics of unsteady flow.

In this article a brief description of the experimental program will be presented followed by a short discussion of the analysis procedures and codes. An overview of the external flow calculations and comparison with flight data will follow in the results section. The majority of the results section will

Presented as Paper 95-2758 at the AIAA/ASME/SAE/ASEE 31st Joint Propulsion Conference and Exhibit, San Diego, CA, July 10–12, 1995; received Sept. 26, 1995; revision received Jan. 3, 1996; accepted for publication Jan. 3, 1996.

*Supervisor, Propulsion Aerodynamics Section, 2001 Aerospace Parkway. Senior Member AIAA.
†Senior Engineer, Propulsion Aerodynamics Section, 2001 Aerospace Parkway.
‡Aerospace Engineer, Inlet and Propulsion Airframe Integration Technology Branch, 21000 Brook Park Road.
§Senior Engineering Associate, Computational and Graphics Support Section, 2001 Aerospace Parkway.

focus on an evaluation of the computational results for the inlet flowfield using the flight data. Following this, the major conclusions of this study will be reviewed. Further details can be found in Refs. 10 and 11 for several angles of attack and Mach numbers.

Experimental Program

The flight data were obtained using a specially equipped F/A-18A aircraft called the High Alpha Research Vehicle. This aircraft has several rows of static pressure taps located at several axial stations along the fuselage and LEX upper and lower surfaces. The inlet highlight region and duct contained low-response (67 Hz) and high-response (2143 Hz) static pressure probe pairs located at several circumferential and axial locations. At the engine face, a rake consisting of 40 low- and high-response total pressure probe pairs distributed on an equal area basis were used to measure the total pressure distortion as a function of time. Further details of the data acquisition process are contained in Ref. 10. The corrected mass flow rate for the inlets is 144 lbm/s.

Numerical Modeling

NPARC Code

The NPARC code, version 2.0 (Ref. 12) solves the full three-dimensional Reynolds-averaged Navier–Stokes equations in strong conservation form using the Beam and Warming approximate factorization scheme to obtain a block tridiagonal system of equations. Pulliam's scalar pentadiagonal transformation provides for an efficient solver. The code uses the Baldwin–Lomax turbulence model,[13,14] along with several other models, which include the RNG,[15] Baldwin–Barth,[16] and κ-ε (Ref. 17) turbulence models. The calculations presented in this study were done using the Baldwin–Barth turbulence model. The implicit scheme uses central differencing with artificial dissipation to eliminate oscillations in the solution associated with the use of central differences. The code allows the use of multiple grid blocks. Trilinear interpolation[18] is used to transfer information at the grid block interfaces.

The second- and fourth-order artificial dissipation factors were set at their default values (0.25 and 0.64, respectively). In general, the variable time step limiter (DTCAP) for viscous blocks was set to a value of 1.0, and for inviscid blocks, 5.0.

Boundary Conditions

The far-field-type boundary conditions were imposed along the outer computational boundaries. This type of condition uses a one-dimensional Riemann invariant to maintain the freestream flow conditions. Along the windward side of the airframe, no-slip, adiabatic conditions are specified. Along the leeward side of the aircraft, inviscid flow is specified. The use of inviscid flow approximation along the upper surface reduced the grid density requirements significantly. No difficulties were encountered along the viscous and inviscid interfacing boundaries. The static pressure at the engine face was adjusted to obtain the rake corrected mass flow rate (144 lbm/s) based upon total pressure at the engine face plane obtained from an average of 40 total pressures in a configuration of eight equally spaced legs with five equal area total pressure locations per leg. This is the flow rate to be obtained in the flight tests. Symmetry conditions are assumed along the centerline of the aircraft.

Grid Generation

Accurate modeling of the geometry and judicious clustering of grid points are needed for a correct numerical simulation and an economical computation. The complex, multiblock grid that was used for these calculations, and was very effective, was created with the GRIDGEN version 6.0 grid generation system.[19]

The geometry is shown in Fig. 1. Complex interactions between the fuselage flowfield and the inlet flowfield, required the inclusion of the forebody, fuselage, LEX, ramp, and wing in the grid. The horizontal tail, vertical tail, aft fuselage, and nozzle were not modeled because they have minimal effects on the inlet flowfield. The wing leading-edge flap is deflected for 30- and 60-deg angle of attack, which is consistent with the actual flight vehicle. An embedded c-grid about the inlet highlight region is also included to improve the resolution of flow gradients and surface geometry. A pair of vortex generators that are positioned approximately halfway downstream in the inlet were not modeled because of their small size and minimal effects on the flowfield at high angles of attack. The vortex generators are ineffective because they are submerged in the boundary layer and do not provide adequate mixing of the large regions of low energy associated with flows at high angles of attack.

Having discussed the components of the aircraft included in the computational model, details of the grid are presented. The model consists of 22 grid blocks. The plane of symmetry and surface grids are shown in Fig. 2. The grid consists of approximately 1.1 million points. The forebody, lower LEX surface, and inlet duct grids were used to compute the viscous flow with a y^+ grid spacing off the wall of approximately 1. The grids above the LEX and along the fuselage aft of the inlet were used to calculate inviscid flow and were much coarser. The viscous effects were deemed significant for the inlet performance calculations ahead of the inlet and under the LEX.

A complete summary of the grid block dimensions is available in Ref. 11. The outer flowfield boundaries were approximately one body length away from the aircraft.

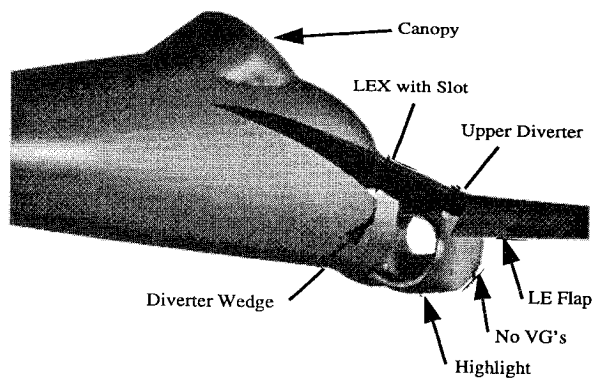

Fig. 1 F/A-18A geometry.

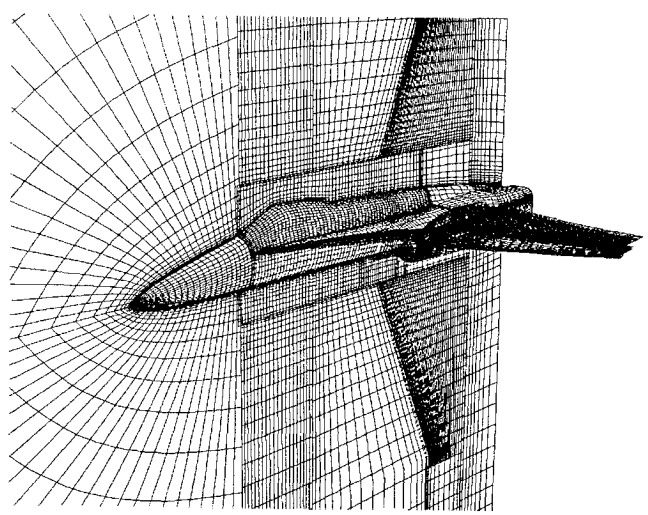

Fig. 2 F/A-18A surface and plane-of-symmetry grid.

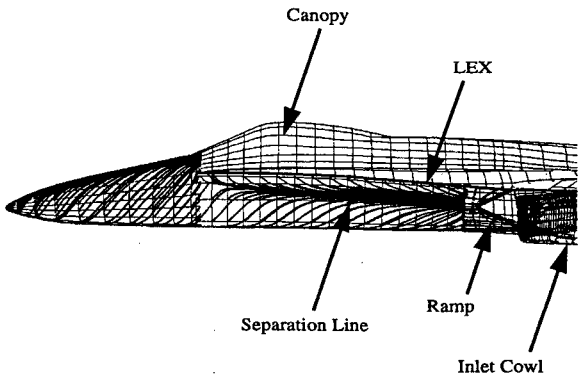

Fig. 3 Surface particle traces (M_∞ = 0.3, α = 30 deg, β = 0 deg).

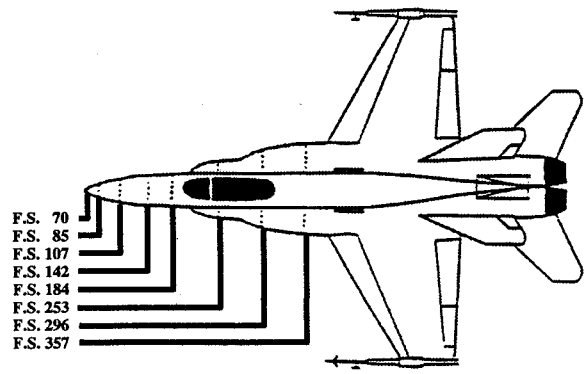

Fig. 4 Forebody/LEX surface pressure measurement stations.

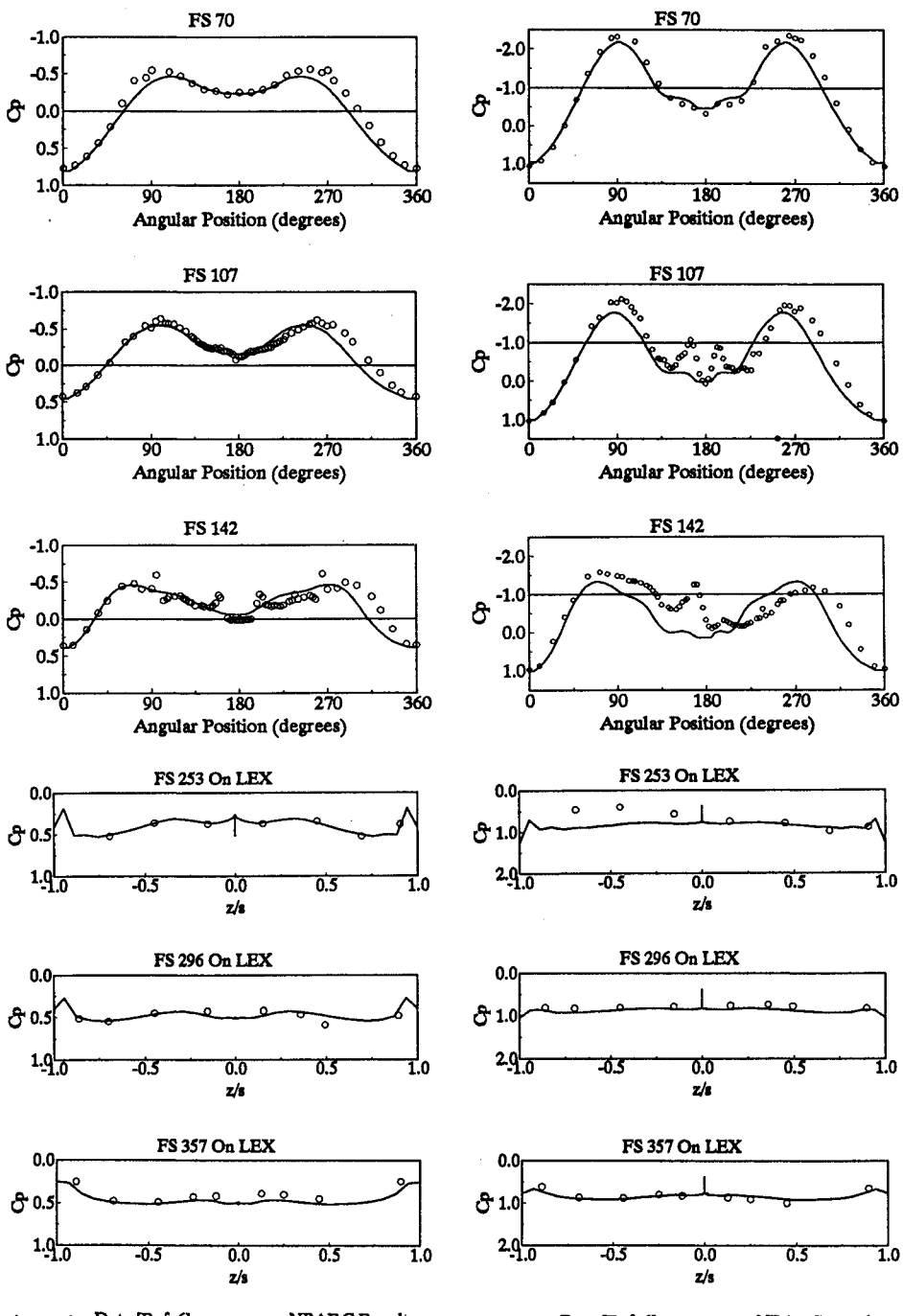

Fig. 5 Forebody/LEX surface static pressure distributions: a) M_∞ = 0.3, α = 30 deg, β = 0 deg and b) M_∞ = 0.3, α = 60 deg, β = 0 deg.

Results

External Flow

In this section the details of the external flowfield are presented. The cases chosen are 30- and 60-deg angle of attack, 0-deg angle-of-yaw, and a freestream Mach number of 0.3. Further details are found in Ref. 11. The graphical results in this section were obtained with the PLOT3D code.[20]

The predicted particle traces (simulated oil flows) along the forebody and fuselage under the LEX are shown in Fig. 3. A windward vortex is generated when the flow impinges on the bottom of the LEX and moves down the fuselage until it reaches a separation line. Surface static pressure data from flight tests[7] were taken at several fuselage stations as shown in Fig. 4. These tests were performed to study external aerodynamic problems. The data are included here to validate the external flow calculations that are needed to provide the proper flow into the inlet. The numerical results for the surface static pressures along the forebody and under the LEX are in good agreement with the data, as shown in Fig. 5. Looking downstream 0 deg is the bottom of the fuselage, 90 deg is the right side, and 180 deg is the top. The flight conditions are the same as those for the particle traces. Discrepancies between the numerical results and data may be because of inadequate grid resolution of the vortex-dominated flow. Also, laminar-to-turbulent transitioning flow, which is present in the flight data, may be a contributing source. The calculations assumed fully turbulent flow present everywhere. Along the top side of the LEX (not shown) the agreement is poor because of a lack of adequate grid resolution and the use of the inviscid flow approximation in this region. Since this region is shielded by the LEX from the inlet, it is assumed to have a minimal effect on the inlet flowfield.

In summary, the predicted flow about the forebody was in good agreement with the data, especially at 30-deg alpha. At 60-deg alpha, there was a small amount of departure as the vortex developed along the forebody. This may indicate a need for further grid refinement to resolve the vortex development. However, since this flow is not ingested by the inlet, but moves over the top of the aircraft, more accurate resolution of the vortical flowfield will not affect the inlet flowfield calculations.

Internal Flow

From an examination of the predicted particle trajectories (not shown) from under the LEX and into the inlet several observations were made. At 60-deg angle of attack, the LEX vortex migrates to the engine face near the center of the duct. Since the total pressure rake has no probes in this region, the distortion caused by the ingested vortex cannot be verified. For 30-deg angle of attack, the ingested vortex does not migrate to the engine face, but dissipates upstream. This observation is supported by the lack of a second low-pressure region in the experimental total pressure contours. There is no significant vortex development under the LEX for 3-deg angle of attack.[11]

The inlet highlight and duct surface pressures are shown in Fig. 6 for 30- and 60-deg angles of attack and 0.3 Mach number. Looking downstream, the 0-deg position is at the top of the inlet entrance, 90 deg is the outboard horizontal position, 180 deg is the bottom of the entrance, and 225 deg is near the lower inlet/fuselage junction. The comparison of the data with the NPARC results indicates two major points. The first one to note is the NPARC results miss some of the peaks in the pressure diagrams about the highlight region. This may be because of a lack of adequate grid resolution in this region. The second point is at 30- and 60-deg angle of attack and 0.3 freestream Mach number, where the pressure data indicate a possible flow separation at the 180-deg station of the inlet lip by the significantly reduced slope of the experimental pressure diagram. In contrast, the NPARC results show a rapid deceleration in this same region, indicating the flow is attached. The

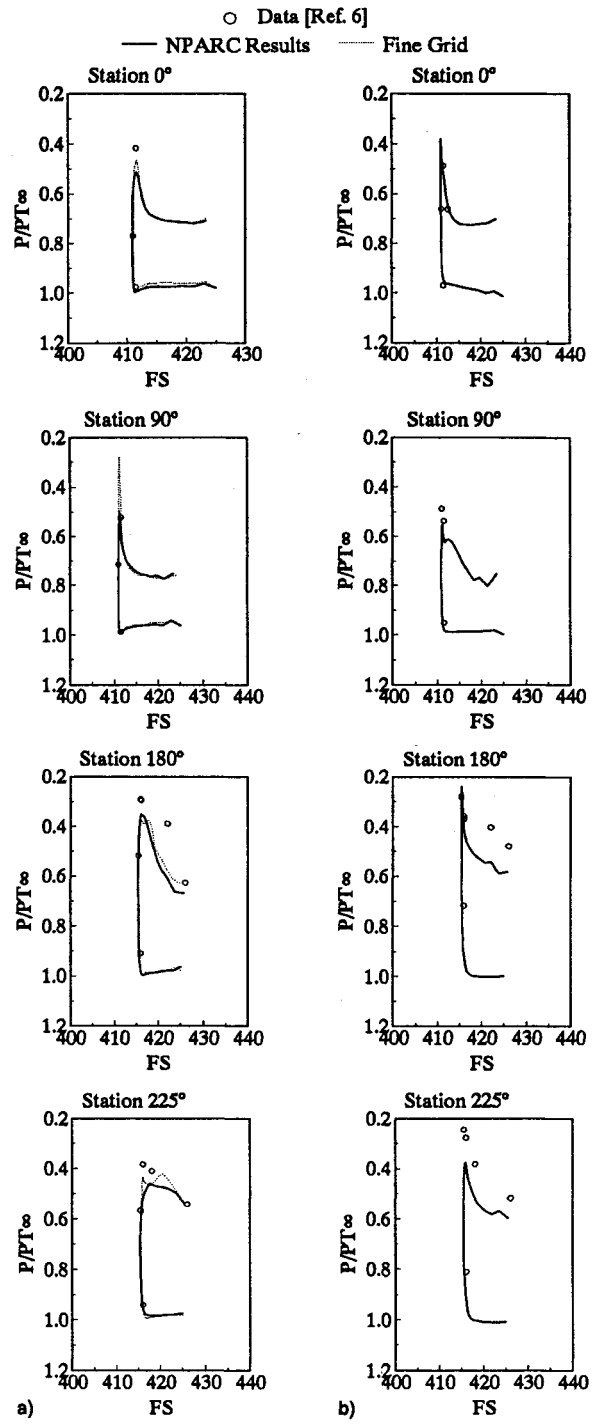

Fig. 6 Inlet highlight surface pressures: a) $M_\infty = 0.3$, $\alpha = 30$ deg, $\beta = 0$ deg and b) $M_\infty = 0.3$, $\alpha = 60$ deg, $\beta = 0$ deg.

results of doubling the inlet lip grid block dimensions in all directions are compared to the present grid in Fig. 6a. The static pressure distributions obtained with the fine grid indicate that the minimum pressure at station 0 deg was closer than the present grid. However, along the lower portions of the highlight (station 180 and 225 deg), the fine grid results were very similar to the present grid. Since the data indicate a thickening boundary layer, a deficiency in the turbulence model may be the source of the discrepancies between NPARC results and data.

Having discussed the inlet highlight region pressures, the circumferential pressure distribution at the engine face will be examined. A comparison of the flight data with the NPARC results is shown in Fig. 7 for 30- and 60-deg angles of attack

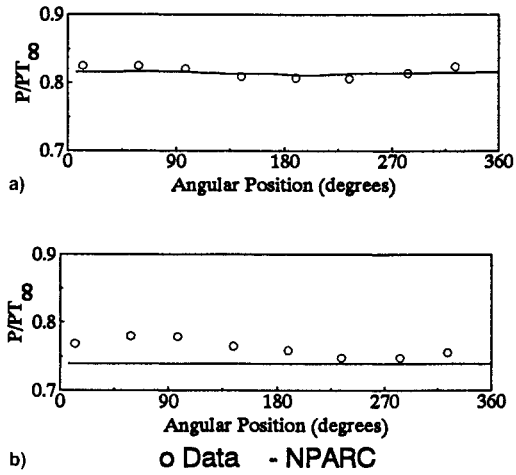

Fig. 7 Engine face circumferential surface pressures: a) $M_\infty = 0.3$, $\alpha = 30$ deg, $\beta = 0$ deg and b) $M_\infty = 0.3$, $\alpha = 60$ deg, $\beta = 0$ deg.

and 0.3 Mach number. It is important to note that the NPARC boundary condition at the engine face was an extrapolation of the static pressure gradient. This gradient was scaled by a single pressure value to adjust the mass flow rate to the desired value. The exception to this was the 60-deg angle-of-attack case in which a constant uniform static pressure was applied. This was done because of streamwise flow separation occurring with the extrapolated pressure gradient boundary condition. The circumferential pressure gradients determined by NPARC are only because of pressure gradients that develop within the duct without any simulation of the influence of the engine. The experimental pressure gradients are very small with the exception of 60-deg angle of attack, and similar to the computational results with the exception at 60-deg angle of attack. For the 60-deg angle-of-attack case, the extrapolation of the static pressure gradient may have improved the agreement between the data and the NPARC results.

The comparison of the NPARC predicted total pressure contours at the engine face with experimental unsteady data is shown in Fig. 8 for 0.3 Mach number and 30- and 60-deg angles of attack. The total pressure contours showing the limits of the migration of the low total pressure region were obtained using the General Electric High Alpha Program (HAP). Each time slice (1/2143 s) of total pressure data was placed in a PLOT3D flow file with the rake total pressure probe coordinates in a PLOT3D grid file. Time was treated as the x axis in the FAST program.[21] The migration of the low total pressure region was examined by moving through time along the x axis using the FAST program. The extremes in movement of the low total pressure region were used to determine which time slices to plot with the HAP program. An examination of predicted vector plots (not shown) indicates that this low total pressure region represents the position of the inlet duct secondary flow vortex for 30- and 60-deg angles of attack.

Several issues are pointed out from studying the comparison of the NPARC results with the flight data. The comparison of the NPARC results with the data indicates a qualitative agreement with the data in terms of the general flow structure. The position and strength of the predicted low total pressure region are different from the data because of the unsteady nature of the flowfield, as shown in the accompanying total pressure contours. These indicate the extent of the migration of the low total pressure region as a function of time. The strength (total pressure loss in this region) also varied with time. The NPARC results fall within the migration range of this region. The NPARC asymptotic solution represents a snapshot of the dynamic flowfield, which is at an arbitrary point in time fixed by the boundary conditions imposed. Therefore, the best obtainable solution is one that lies within the excursion of the unsteady flowfield. To perform an unsteady flow analysis an unsteady engine face boundary condition may be required. From observing the experimental total pressure contours at the engine face as a function of time, the flowfield appears to change in a random way, requiring a statistical or probability representation of the pressure field at the engine face. The migration range of the vortex or low total pressure region increased with increasing levels of distortion. This indicates that the flow becomes more unsteady as the distortion levels increase. Also, the presence of the engine may have a significant effect on the movement of the secondary flow vortex. A suggested research area would be to model a shedding vortex from a cylinder using an unsteady and asymptotic solution and examine the effects of a steady-state approximation on the unsteady flowfield.

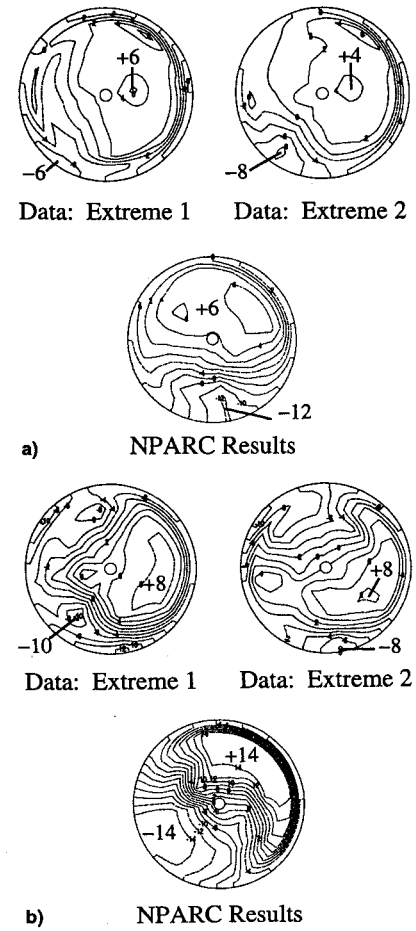

Fig. 8 Engine face normalized total pressure contours $(P_T - P_{T_\infty})/P_{T_\infty}$: a) $M_\infty = 0.3$, $\alpha = 30$ deg, $\beta = 0$ deg and b) $M_\infty = 0.3$, $\alpha = 60$ deg, $\beta = 0$ deg.

In summary, the inlet lip region flow calculations indicate a need for improved modeling of the separated flows. The Baldwin–Barth turbulence model did not adequately resolve the possible lower lip flow separation. Overall, the vortical flow within the inlet duct was simulated reasonably well in terms of the results falling within the limits of the actual unsteady flow. The Baldwin–Barth turbulence model overpredicts the strength of the secondary flow vortex in terms of a region of lower total pressure than the data.

A comparison of the predicted inlet performance to the experimental data is shown in Table 1. The data are for the minimum to maximum values obtained in the experimental sample group, whereas the NPARC results are for an arbitrary instantaneous point in time as previously discussed. In general, the recoveries and distortions calculated from the NPARC results are at the high loss end of the data range. Since the actual flow is very unsteady, the value of these types of comparisons is difficult to assess.

Table 1 Inlet performance summary

	α = 30 deg		α = 60 deg	
M_∞ = 0.3	NPARC	Data	NPARC	Data
$\dot{m}_{corr}$, lbm/s	143.3	145.8	143.7	145.9
Recovery, %	95.1	97–98	88.5	90–92
Distortion, %	19.0	9–13	31.5	14–28

Numerical Issues

For such a complex problem, determining the convergence of the solution is not a straightforward task. Residuals are not very reliable since they tend to drop a few orders of magnitude and then level off for complex viscous flows. Therefore, we follow the flow quantities of interest as the solution iterates to determine when these quantities stop changing or the changes per iteration become insignificant. Several quantities are presented for convergence criteria in the following discussion.

The calculated forces on the aircraft served as one measure of convergence of the external flowfield. The predicted lift and drag coefficients varied by less than 1% as the solutions were converged. The surface static pressure distributions maintained nearly constant values as the solution was iterated. For the inlet duct flow, the variation in mass flow rate at each axial computational station was compared to the entrance value. The variation was within 1% of the entrance values.

The grid and input file generation required approximately two months to complete, with additional time spent on grid refinements. A typical solution required from 50 to 75 Cray Y-MP CPU hours, using a previous solution for a starting solution. An initial solution starting with freestream conditions may require at least 100 Cray Y-MP CPU hours.

Conclusions

The results of this study indicate several important conclusions. The first one is the need to include the external airframe in the calculations of the flow within the F/A-18A inlet because of the high degree of integration of the inlet with the airframe. As the angle of attack increased, more of the external flow impacted on the inflow to the inlet with regard to the under LEX vortex ingestion and its effect on the total pressure distortion pattern at the engine face. The NPARC results compared well with the forebody and lower LEX surface static pressures, which indicates that the pertinent aspects of the external flowfield were modeled well for the inlet flowfield simulation.

The effects of the inlet highlight are also very important to the inlet flowfield. The measured surface pressures along the highlight were in good agreement, in general, with the NPARC results. Possible flow separation shown in the data was not present in the numerical results along the lower region of the highlight. The effects of the presence of the engine appear to be small with regard to the surface circumferential pressure distribution at the engine face. The NPARC predictions agreed well with the flight data. It is unknown how significant the presence of the engine is on the migration of the secondary flow vortex or the unsteadiness of the flowfield.

Although the NPARC results represent an asymptotic solution, it was able to capture the essential steady-state physics associated with the inlet flowfield, which is inherently unsteady.

Acknowledgments

Support of this work by the NASA Lewis Research Center under Contract NAS3-27186 is gratefully acknowledged. Interest shown by Project Manager, Thomas Biesiadny, is particularly appreciated. Thanks also to June Thompson of NASA Lewis for her contributions to setting up the data analysis system. In addition, the authors express their appreciation to Tammy Langhals and Maryann Johnston for their outstanding work in producing the text and figures for this article.

References

[1]Burley, R. R., Anderson, B. H., Smith, C. F., and Harloff, G. J., "High Alpha Inlets," NASA 10063, March 1991, pp. 5-1–5-14.

[2]Ghaffari, F., Bates, B. L., Luckring, J. M., Thomas, J. L., and Bierdron, R. T., "Navier-Stokes Solutions About the F/A-18 Wing-LEX-Fuselage Configuration with Multi-Block Structured Grids," AIAA Paper 91-3291, Sept. 1991.

[3]Gee, K., Tavella, D., and Schiff, L. B., "Computational Optimization of a Pneumatic Fuselage Forebody Flow Control Concept," AIAA Paper 91-3249, Sept. 1991.

[4]Bruns, J. E., and Smith, C. F., "Installed F/A-18A Inlet Flow Calculations at a High Angle-of-Attack," *Journal of Propulsion and Power*, Vol. 10, No. 1, 1994, pp. 110–115.

[5]Smith, C. F., and Podleski, S. D., "Installed F/A-18A Inlet Flow Calculations: A Grid Study," *Journal of Propulsion and Power*, Vol. 11, No. 6, 1995, pp. 1250–1256.

[6]Podleski, S. D., Smith, C. F., Barankaweiz, W. S., and Zeleznik, S., "Comparison of F/A-18A Inlet Flow Analysis with Flight Data Part 2," *Journal of Aircraft*, Vol. 33, No. 3, 1996, pp. 463–469.

[7]Fisher, D. F., Banks, D. W., and Richwine, D. M., "F-18 High Alpha Research Vehicle Surface Pressures: Initial In-Flight Results and Correlation with Flow Visualization and Wind Tunnel Data," NASA TM 101724, Aug. 1990.

[8]Amin, N. F., Hollweger, D. J., Franks, W. J., de la Vega, E. G., Yamada, M., and Tsukahira, T. W., "AEDC Series 1 F-18, .192 Scale Inlet Analysis Report," Northrop Corp., Aircraft Div., NOR 77-310, Hawthorne, CA, May 1977.

[9]Amin, N. F., Richards, C. J., de la Vega, E. G., and Dhanidina, M. A., "F/A-18A Engine Inlet Survey Report, Vols. 1, 2 and 3," Northrop Corp., Aircraft Div., NOR 81-316, Hawthorne, CA, Nov. 1981.

[10]Smith, C. F., Podleski, S. D., and Barankiewiez, W. S., "Comparison of F/A-18A High Alpha Research Vehicle Inlet Flow Analysis Results with Flight Data: Part I (Without Sideslip)," AIAA Paper 95-2758, July 1995.

[11]Smith, C. F., Podleski, S. D., Barankiewicz, W. S., and Zeleznik, S. Z., "Evaluation of F/A-18A HARV Inlet Flow Analysis Results with Flight Data: Final Report," NASA TM 107130, Dec. 1995.

[12]"A User's Guide to NPARC, Version 2.0," The NPARC Alliance, Arnold Engineering Development Center, Tullahoma, TN, 1994.

[13]Baldwin, B. S., and Lomax, H., "Thin-Layer Approximation and Algebraic Turbulence Model for Separated Turbulent Flows," AIAA Paper 77-257, Jan. 1977.

[14]Sirbaugh, J. R., and Reichart, B. A., "Computation of a Circular-to-Rectangular Transition Duct Flow Field," AIAA Paper 91-1741, June 1991.

[15]Ahn, K. H., "Performance of Renormalized Group Algebraic Turbulence Model on Boundary Layer Transition Simulation," NASA CR 194466, Feb. 1994.

[16]Baldwin, B. S., and Barth, T. J., "A One-Equation Turbulence Transport Model for High Reynolds Number Wall-Bounded Flows," NASA TM 102847, Aug. 1990.

[17]Georgiadis, N. J., Chistsomboon, T., and Zhu, J., "Modification of the Two Equation Turbulence Model in NPARC to a Chien Low Reynolds Number κ-ε Formulation," NASA TM 106710, Sept. 1994.

[18]Stokes, M. L., and Kneile, K. L., "A Search/Interpolation Algorithm for CFD Analysis," World Congress on Computational Mechanics, Univ. of Texas, Austin, TX, Sept. 1986.

[19]Steinbrenner, J. P., Chawner, J. R., and Fouts, C. L., "The Gridgen 3-D Multiple Block Grid Generation System," Wright Research and Development Center, WRDC-TR-90-30222, Wright–Patterson AFB, OH, July 1990.

[20]Walatka, P. P., Buining, P. G., Pierce, L., and Elson, P. A., "PLOT3D User's Guide," NASA TM 101067, March 1990.

[21]Walatka, P. P., Plessel, T., McCabe, R. K., Clucas, J., and Elson, P. A., "FAST User's Manual," NASA Ames Research Center, WAO and RND, Beta 2.0, RND-91-011, Dec. 1991.